Journal of Environmental Chemical Engineering 10 (2022) 107847

Contents lists available at ScienceDirect

Journal of Environmental Chemical Engineering

journal homepage: www.elsevier.com/locate/jece

Non-equilibrium plasma enhanced oxygen vacancies of CuO/CeO_2 nanorod catalysts for toluene oxidation

Jianyu Yun [a], Liangkai Wu [a], Qinglan Hao [a], Zihao Teng [a], Xin Gao [a], Baojuan Dou [a,*], Feng Bin [b,*]

[a] Tianjin University of Science & Technology, Tianjin 300457, China
[b] State Key Laboratory of High-Temperature Gas Dynamics, Institute of Mechanics, Chinese Academy of Science, Beijing 100190, China

ARTICLE INFO

Keywords:
Non-equilibrium plasma
CuO/CeO_2
Oxygen vacancy
VOCs
Catalytic oxidation

ABSTRACT

The development of non-noble metal catalyst is essential for VOCs controlling. Cu-Ce based catalyst is a promising catalyst, and the oxygen vacancies dominants the catalytic oxidation process but the traditional calcination is not conducive to its generation. Herein a series of CuO/CeO_2 nanorod catalysts for toluene oxidation were prepared with non-equilibrium plasma comparing with traditional calcination. It is found that the treatment of non-equilibrium plasma after calcination can significantly enhance the synergism between CuO active phase and CeO_2 support leading to high dispersion of CuO. And the non-equilibrium plasma is favorable to increase Cu^+/Cu^{2+} and Ce^{3+}/Ce^{4+} ratios generating more oxygen vacancies in the catalyst. In the process of toluene oxidation, the rich oxygen vacancy can accelerate adsorption and activation of gaseous oxygen which consequently improve the catalytic activity for toluene oxidation.

1. Introduction

Volatile organic compounds (VOCs) are not only directly endangered to human health, but also significant precursors of ozone and PM2.5 pollutants in the air [1,2], hence the control of VOCs pollution has become the key issue to improve air quality in China. Compared with adsorption, thermal combustion, photocatalysis and other technologies [3–5], catalytic oxidation can decompose VOCs into CO_2 and H_2O completely at low temperature, with high efficiency, no secondary pollutants such as NOx [6], and it is an energy-saving and emission-reduction technology for VOCs controlling to achieve the targets of peak carbon dioxide emissions and carbon neutrality in China.

Catalyst is the key factor of catalytic oxidation technology. At present, Pt and Pd based noble metal catalysts are widely used in the industry, however they are expensive, prone to sinter at high temperature, and are easily poisoned and deactivated when reacting with halogenated organics [7–9]. Therefore, the research and development of highly active non-noble metal catalysts is a research hotspot in the catalytic oxidation of VOCs. Transition metal oxides and their composite oxides have the advantages of low price, strong oxygen storage and release capacity, and good reducibility [10–12]. Among them, the rare earth element Ce has abundant oxygen vacancies and the unique property of the conversion between Ce^{3+} and Ce^{4+}, which make it have excellent oxygen storage and release capabilities. When used as a carrier, Ce can interact with active components to promote catalytic activity [13–16]. Yang P et al.[17] found that part of the active metal ions of the 4Ce1M (M=V , Cr , Mn , Fe , Co , Ni and Cu) can enter the CeO_2 fluorite lattice due to the strong interaction between CeO_2 and MOx, and the redox property of the 4Ce1M catalyst is conducive to complete oxidation and decomposition of Cl-VOCs at a lower temperature. Studies have found that CeO_2 based composite oxides can improve the catalyst's ability to store and transport oxygen, as well as the activity and thermal stability of the catalyst [18,19]. He et al. [20] reported that CuCeOx exhibited the highest degradation efficiency with 99% chlorobenzene oxidation at 328 ℃, comparing with ACeOx (A=Co、Fe、Mn, Zr) catalysts, attributing to the formation of Cu^{2+}-O^{2-}-Ce^{4+} improving the oxidation-reduction ability and realizing an efficient redox cycle reaction. In addition, the oxygen vacancies in the catalyst play an important role in the catalytic oxidation process [21]. Control methods of oxygen vacancy include metal and non-metal doping, reduction, high-temperature calcination and so on. Our previous study demonstrated that the oxygen vacancy content in CuCeOx synthesized by glucose-containing bacterial cellulose was obviously higher than traditional methods [21]. Nevertheless, the traditional high-temperature calcination of CuCeOx could lead to the agglomeration of CuO and inhibit the generation of oxygen vacancies to a certain extent. Therefore,

* Corresponding authors.
E-mail addresses: bjdou@tust.edu.cn (B. Dou), binfeng@imech.ac.cn (F. Bin).

https://doi.org/10.1016/j.jece.2022.107847
Received 17 February 2022; Received in revised form 4 April 2022; Accepted 2 May 2022
Available online 11 May 2022

it is very important to explore new preparation technology to improve the dispersion of active components and concentration of oxygen vacancy for CuCeOx catalyst.

Non-equilibrium plasma provides rich high-energy electrons and active radicals with a strong reduction ability [22,23]. Its "high-energy and low-temperature" characteristic is considered to be one of environmentally friendly, energy-saving and efficient method for the catalyst preparation. The high-energy electrons and active radicals can decompose the catalyst precursor and nucleate metal ions quickly, which is beneficial to avoid sintering and agglomeration of metal particles. Zhang. et al. [24]. found that the dispersion of the Au particles (7–8 nm) and oxygen species content on the carbon surface increased with the treatment of argon glow discharge plasma at ambient temperature. Compared with the traditional catalyst prepared by hydrogen reduction, the Au/C catalyst prepared with plasma exhibited better selective oxidation of glucose. Therefore, it is of great importance to employ on-equilibrium plasma to enhance oxygen vacancy in CuCeOx and activity.

In this study, a series of CuO/CeO_2 nanorods with or without glucose were prepared by the non-equilibrium plasma and traditional calcination, and the process and characteristics of non-equilibrium plasma treating catalyst precursors were studied. Combined with characterizations of X-ray diffraction (XRD), transmission electron microscopy (TEM), Raman, H_2 temperature programmed reduction (H_2-TPR), O_2 temperature programmed desorption (O_2-TPD) and X-ray photoelectron spectroscopy (XPS), the influences of non-equilibrium plasma on the crystal structure and physicochemical properties of the catalyst surface were systematically analyzed. Furthermore, the catalytic performances of toluene oxidation over CuO/CeO_2 were investigated in a fixed bed, and the structure-activity relationship and oxidation reaction mechanism were deeply analyzed.

2. Experimental

2.1. Catalyst preparation

7.82 g of Ce $(NO_3)_3.6\ H_2O$ was dissolved in 160 mL of deionized water, then 80 g of NaOH solid was added into the solution stirring for 30 min. Then the solution was transferred into a 200 mL hydrothermal reactor and reacted at 100 °C for 12 h. After cooling to room temperature, the solid was washed until the supernatant was neutral, followed by drying at 80 °C for 12 h. A long rod-shaped CeO_2 carrier was obtained after calcination at 450 °C for 5 h.

A certain amount of Cu $(NO_3)_2$•3 H_2O with a molar ratio of CuO: CeO_2 = 1:5 was dissolved in distilled water containing 0% and 2% glucose, respectively. Then the prepared CeO_2 rod was impregnated in the above mixed solution for 12 h by an equal volume immersion method, and the catalyst precursor was obtained after drying at 80 °C for 6 h. The catalyst precursor was calcined at 450 °C for 2 h, and the obtained catalysts with and without glucose were marked as CuCe-SC and CuCe-C, respectively.

The plasma treatment of catalyst was carried out in a coaxial cylindrical plasma reactor, which was made of quartz glass tube with an inner diameter of 19 mm and wall thickness of 3 mm wrapped by the copper mesh of 5 cm length as a ground electrode. The inner discharge electrode was tungsten wire (10 mm in diameters) placed on the axis of the reactor. AC power supply (CTP-2000 K, 3–100 kHz, 0–100 kV). The catalyst was treated by non-equilibrium plasma for about 20 min under the voltage of 7.6 kV and frequency of 9.85 kHz. The catalysts precursor after treatment of non-equilibrium plasma were marked as CuCe-P (without glucose) and CuCe-SP (with glucose). The catalyst precursor was calcined at 450 °C and then treated by plasma, and the prepared catalysts were labeled as CuCe-CP (without glucose) and CuCe-SCP (with glucose).

2.2. Characterization

XRD pattern was recorded on XRD-6100 X-ray powder diffraction analyzer with light source of Cu Kα (λ = 0.1540560 nm) and scanning speed of 0.02°/min. TEM were acquired on a Philips Tecnai G2 F20 transmission electron microscope. Raman spectrum was conducted by HORIBA LabRAM HR Evolution equipped with a 488 nm laser. XPS was measured on a Perkin-Elmer PHI-1600 spectrometer with a Mg Kα X-ray source (1253.6 eV) calibrated by an internal standard of C 1 s at 284.8 eV. H_2-TPR tests were carried out on PCA-140 instrument (TP-5080B), 20 mg of catalyst was pretreated with Ar (30 mL/min) at 300 ℃ for 30 min, and then 5% H_2/Ar (30 mL/min) was introduced to reduce the catalyst from room temperature to 600 °C at 10 ℃/min. O_2-TPR experiment was performed on the same PCA-140 instrument with 50 mg of catalyst used for the determination. After pretreatment with N_2 (30 mL/min) at 300 °C for 30 min, the catalyst was allowed to adsorb O_2 (30 mL/min) at 50 °C for 30 min, and then purged with N_2 (30 mL/min) for 30 min. Then the temperature increased from room temperature to 700 °C with a heating rate of 10 ℃/min, and the O_2 consumption was detected by thermal conductivity (TCD) detector. The FTIR spectroscopy was obtained by a Bruker Tensor 27 spectrophotometer.

2.3. Activity evaluation of catalyst

As a typical VOCs, toluene was selected as the target pollutant, and the evaluation of catalyst activity for toluene oxidation was carried out in a fixed-bed reactor [21]. 0.8 g catalyst (20–30 mesh) was loaded into the reactor (ϕ8 mm × 1 mm, L=400 mm). The concentration of toluene in the reaction gas was 1000 ppm balanced by dry air with a total gas flow of 300 mL/min, space velocity (SV) of 18000 h^{-1}. The gas composition before and after the reactor were analyzed by a gas chromatograph (GC, Shimadzu). The flame ionization detector (FID, DB-35MS) and TCD (AE. Porapak N) in GC were used to quantitatively analyze toluene and CO_2, respectively. The oxidation efficiency of toluene was calculated based on the concentration change between inlet and outlet gas. CO_2 selectivity was obtained as a percentage of the CO_2 concentration in outlet to the total content of CO_2 from theoretical conversion of toluene.

3. Results and discussion

3.1. Characteristics of non-equilibrium plasma during CuO/CeO_2 preparation

The treatment of non-equilibrium plasma for the catalyst was performed in a quartz glass reactor via dielectric barrier discharge in air. the catalyst was treated by non-equilibrium plasma for about 20 min under the stable discharge. The experimental phenomenon of gas discharge when CuO/CeO_2 catalysts are treated by non-equilibrium plasma is shown in Fig. 1. For the glucose-free catalyst precursor of CuCe-P processed by pure non-equilibrium plasma (Fig. 1A), the discharge is stable during the whole process of nitrate decomposition in the catalyst, with no breakdown phenomenon. Due to the presence of glucose in the catalyst precursor of CuCe-SP (Fig. 1B), pure non-equilibrium plasma treatment easily causes breakdown during gas discharge. Fig. 1B1, B2 and B3 are the photographs of stable discharge, breakdown and post breakdown, respectively. In the early stage of non-equilibrium plasma treatment of CuCe-SP precursor, nitrate is slowly decomposed under the reaction of high-energy electrons, O·, N·and other active radicals, resulting in relatively stable discharge (Fig. 1B1). With the increase of internal temperature of the catalyst, the decomposition of nitrates is accelerated, and the glucose in the precursor also begins to decompose and accumulate heat, which leads to the local temperature of the catalyst being too high and the breakdown phenomenon (Fig. 1B2). The local flying temperature in the catalyst can cause rapid oxidation of partial catalyst and even surface CuO sinter (Fig. 1B3). After the

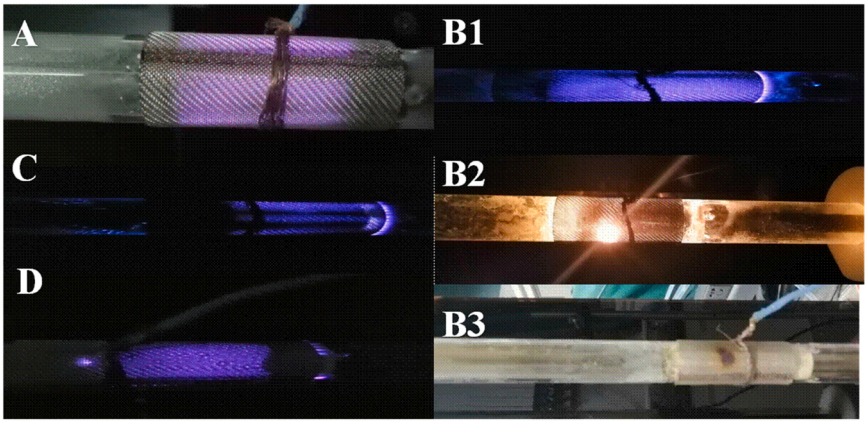

Fig. 1. Experimental phenomenon of gas discharge during non-equilibrium plasma treatment of catalysts. (A: CuCe-P, B: CuCe-SP, C: CuCe-CP, D: CuCe-SCP).

complete decomposition of nitrate and glucose in the precursor, the discharge is gradually stabilized. After calcination at 450 °C, following treatment of non-equilibrium plasma are shown in Fig. 1C and D, respectively. Compared with pure treatment of non-equilibrium plasma, the gas discharge of the combination of calcination and non-equilibrium plasma is more stable. It is obvious that the decomposition of the nitrate and glucose in the catalyst precursor by pure non-equilibrium plasma is likely to cause a large amount of local heat accumulation, which is not conducive to the dispersion of the CuO active phase. It can be concluded that non-equilibrium plasma combined with calcination is the optimal strategy for CuO/CeO_2 preparation.

3.2. FTIR

The FTIR technique was used to analyze the surface functional groups of the CuO/CeO_2 nanorod catalysts under different preparation conditions, and the results are shown in Fig. S1. The bands in the range of 1530–1480 cm^{-1} and 1650–1600 cm^{-1} are assigned to monodentate nitrates and bridge nitrate [26,27], respectively. And the bands in 1153–1082 cm^{-1} region are associated with the stretching vibration of C-O bond [25]. It can be seen from the figure that the correlation peak of nitrate in CuCe-P obtained by pure non-equilibrium plasma treatment is the strongest comparing with other catalysts. It can be explained by the fact that the complete decomposition of the nitrate cannot be achieved simply by non-equilibrium plasma, resulting in some nitrate remaining in the catalyst. With the presence of glucose in catalyst precursor, glucose decomposition by direct non-equilibrium plasma can accumulate energy rapidly and raise the temperature (Fig. 1B), contributing to more decomposition of nitrate in CuCe-SP.

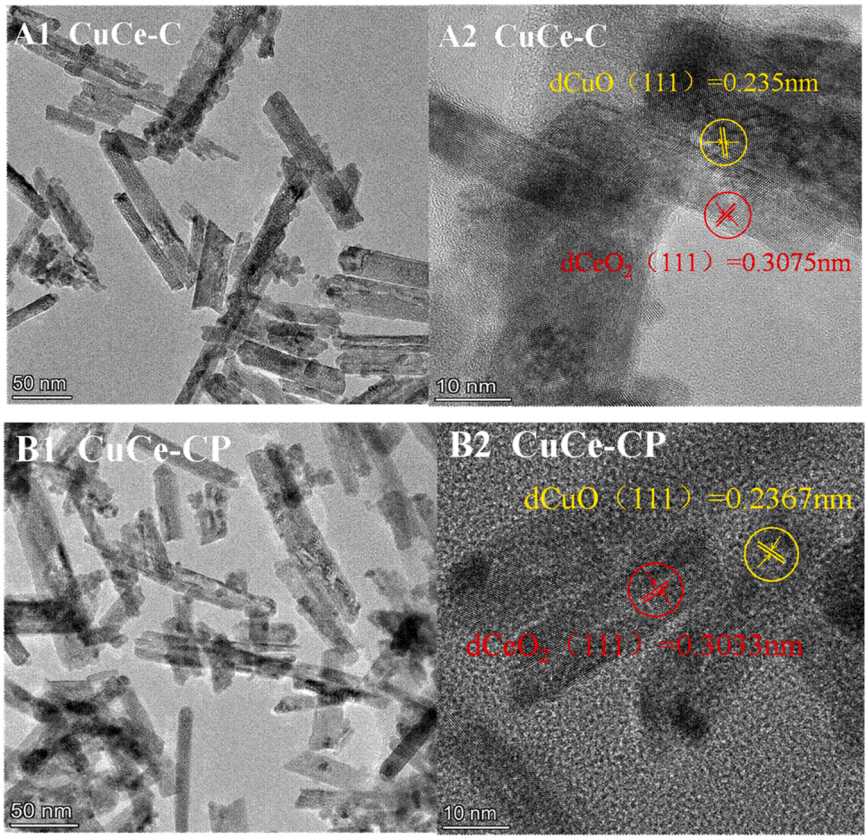

Fig. 2. TEM and HRTEM images of CuCe-C (A1, B1) and CuCe-CP (A2, B2).

3.3. XRD

Fig. S2 shows the XRD patterns of CuO/CeO_2 catalysts obtained under different preparation conditions. It can be seen that all catalysts exhibit a typical CeO_2 (JCPDS#43–1002) fluorite structure with peaks located at 28.5° (111), 33.1° (200), 47.5° (220), 56.3° (311), 59.1° (222), 69.4° (400), 76.7° (331) and 79.1° (420), indicating that the crystal structure of CeO_2 carrier is stable and can be well-maintained after loading of CuO. Besides, weak diffraction peaks emerging at 35.5° and 38.7° correspond to the (111) and (002) planes of CuO, respectively, which suggests that loaded CuO with low crystallinity is well-dispersed on the CeO_2 surface.

3.4. TEM

As shown in Fig. 2, both CuCe-C and CuCe-CP catalysts exhibit regular long rod-like morphologies with exposing CeO_2 (111) and (220) crystal planes and CuO (111). It is obvious that, compared with CuCe-C prepared by conventional calcination, the dispersion of CuO on CuCe-CP is significantly improved due to the treatment of non-equilibrium plasma coupled with calcination, which can inhibit the agglomeration of CuO during the decomposition process of the catalyst precursors [28]. This will further effectively promote the activities of CuO/CeO_2 catalysts. By measuring the lattice spacing, it is found that the lattice fringes of CuCe-C and CuCe-CP can be divided into two types: $dCeO_2(111) = 0.3075$ nm and $dCuO(111) = 0.235$ nm for CuCe-C (Fig. A2), and $dCeO_2(111) = 0.3033$ nm and $dCuO(111) = 0.2367$ nm for CuCe-CP (Fig. B2), both of which deviate from the standard CeO_2(111) and CuO(111). It can be explained by the fact that Cu^{2+} inserted into the lattice structure of CeO_2 causes lattice distortions, which in turn reduces the redox potential of Cu species and promotes the formation of oxygen vacancies around Cu^{2+} [29].

3.5. Raman

The Raman spectra and oxygen vacancy concentration of CuO/CeO_2 nanorod catalysts are shown in Fig. 3. All the results can be marked as four peaks of α, β, γ and δ. The β peak at 452–463 cm^{-1} is attributed to the triple F_{2g} vibration of oxygen atoms in the CeO_2 fluorite structure, which shifts slightly to the left compared with the pure CeO_2 peak (463 cm^{-1}) in other reports [30], suggesting that the addition of Cu^{2+} leads to lattice distortion to varying degrees. The Raman shift is found to be related to the grain size, and the smaller grain corresponds to the more peak shifts to the lower wavenumber [31,32]. It can be seen from Fig. 3(A) that, compared with the glucose-containing catalysts, all the β peaks of glucose-free catalysts shift to the lower wavenumber, proving smaller grain sizes of glucose-free catalysts.

The α peak belongs to the displacement peak of oxygen atoms with crystal structure defects in CeO_2. The γ peak is characteristic of the oxygen vacancies (O_v) which can be promoted by Ce^{3+}, and the δ peak is ascribed to the A_{1g} asymmetric vibration of CeO_2. The relative intensity ratio of the γ peak and the β peak is associated with the concentration of surface oxygen vacancies in the catalysts [33]. The high concentration of oxygen vacancy is beneficial to the adsorption and activation of gas oxygen and thus promotes the catalytic activity. It is noteworthy from Fig. 3B that the glucose-containing catalysts prepared by different methods own lower oxygen vacancy concentrations than corresponding glucose-free catalysts, revealing that the introduction of glucose restrains the generation of oxygen vacancies. The reason may be that glucose cannot be completely decomposed during calcination at 450 °C in this study [34], which hinders the formation of oxygen vacancies. Moreover, the highest content of oxygen vacancies in CuCe-CP also demonstrates that non-equilibrium plasma coupled with calcination can significantly facilitate the oxygen vacancies among all the methods in that it increases the concentration of Ce^{3+}, which has a strong capacity of storing oxygen and generating oxygen vacancies, further leading to such a result. Higher oxygen vacancy concentration can effectively improve the activation and fluidity of oxygen species, contributing to more gas-phase oxygen adsorbed on the catalyst surface, activated into active lattice oxygen and reacted with the adsorbed toluene molecules.

3.6. XPS

The surface compositions and chemical states of the catalysts were studied by XPS. The XPS spectra of Cu, Ce, and O species of CuCe-C, CuCe-P, and CuCe-CP are shown in Fig. 4. The Cu 2p spectrum in Fig. 4A can be fitted to four characteristic peaks of Cu $2p_{3/2}$ (934.6 eV, 942.6 eV) and Cu $2p_{1/2}$ (954 eV, 963.5 eV). Among them, peaks at 934.6 eV and 954 eV are attributed to Cu^{+}, while peaks around 942.6 eV and 963.5 eV belong to Cu^{2+}, proving that Cu^{+}/Cu_2O and Cu^{2+}/CuO species coexist in the catalyst. In Fig. 4B, Ce $3d_{5/2}$ and Ce $3d_{3/2}$ are labeled as v and u, respectively. The u_2 and v_2 peaks at the binding energies of 902.5 eV and 884.9 eV correspond to the Ce^{3+} species due to the lattice defects caused by copper ions entering the CeO_2 lattice [29,35]. Four strong peaks of u_4 (917.5 eV), v_4 (898.4 eV), u_3 (908.1 eV) and v_3 (889.6 eV) and two weak peaks of v_1 (883.9 eV) and u_1 (900.7 eV) are the characteristic peaks of Ce^{4+}. In the O 1 s spectrum (Fig. 4C), the distinctive peaks at 529.3 eV and 531.4 eV represent the oxygen in lattice (O_L) and the chemisorbed oxygen (O_a), respectively. The existence of O_a indicates that gas-phase oxygen is adsorbed on the oxygen vacancies on the catalyst surface [36], and high ratio of O_a reflects high oxygen vacancy concentration. It can be seen from Table 1 that CuCe-CP exhibits the highest concentration of oxygen vacancies, testifying that non-equilibrium plasma coupled with calcination facilitates the formation of oxygen vacancies on the catalyst surface, which is consistent with the results of Raman. As has been stated before, oxygen vacancies can activate gas-phase oxygen, promote the electron transferring and adjust or change the distribution of electrons on the catalyst surface, thereby

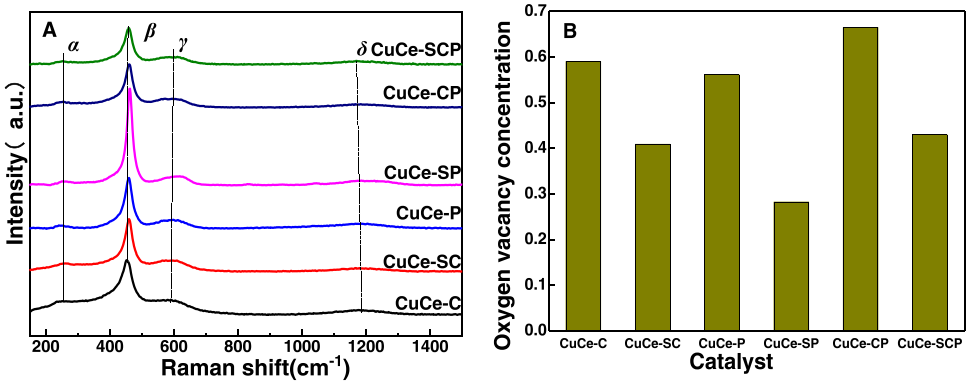

Fig. 3. Raman spectra (A) and oxygen vacancy concentration (B) of catalysts.

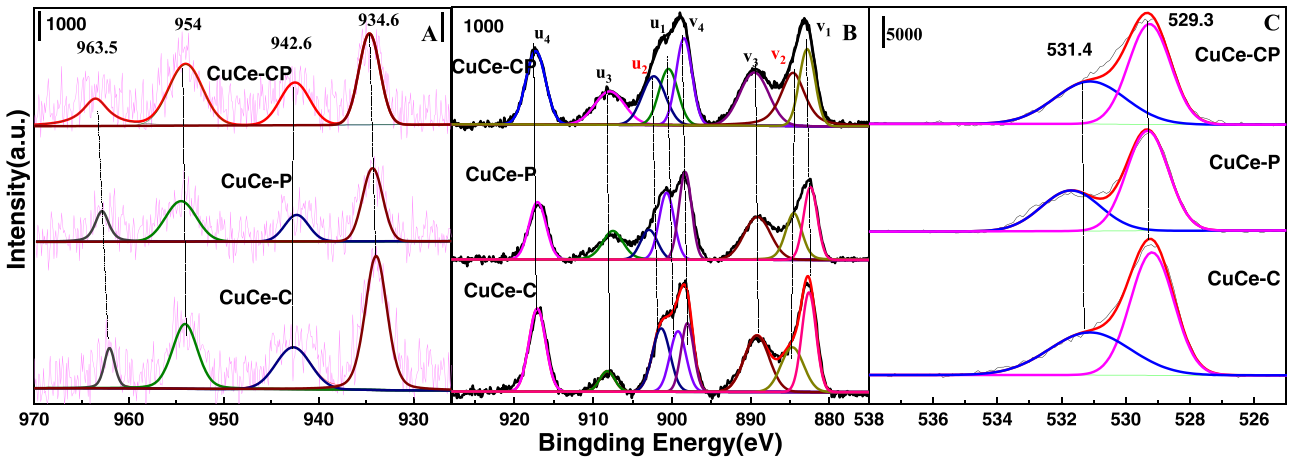

Fig. 4. XPS spectra of CuCe-C, CuCe-P, CuCe-CP (A) Cu 2p; (B) Ce 3d; (C) O 1 s.

Table 1
Surface composition and relative content of CuCe-C, CuCe-P, CuCe-CP, Temperature and peak area of each reduction peak of the catalyst.

Catalyst	Cu^{+}/Cu^{2+}	$Ce^{3+}/(Ce^{3+}+Ce^{4+})$	O_a/O_L	Surface element Composition (%)			H_2-TPR (Position (℃) / Hydrogen consumption (mmol/g))		
				Cu	Ce	O	Peak α	Peak β	Peak γ
CuCe-C	2.58	0.25	0.65	12.96	73.85	13.19	135/0.11	171/0.04	174/0.73
CuCe-SC	–	–	–	–	–	–	136/0.12	149/0.03	176/0.69
CuCe-P	2.33	0.19	0.57	12.93	71.96	15.11	138/0.21	168/0.08	175/0.74
CuCe-SP	–	–	–	–	–	–	139/0.29	162/0.13	175/0.49
CuCe-CP	2.72	0.27	0.71	12.84	72.74	14.42	130/0.14	142/0.07	172/0.64
CuCe-SCP	–	–	–	–	–	–	143/0.19	162/0.04	184/0.73

improving the catalytic activities [37]. CuCe-CP possesses the highest content of Ce^{3+}, which can benefit the formation of oxygen vacancies, the storage of a large amount of oxygen and the redox ability and activity of the catalysts. Meanwhile, from Fig. 4A and Table 1, it is shown that CuCe-CP exhibits the highest ratios of Cu^{+}/Cu^{2+} (2.72) compared with CuCe-C (2.58) and CuCe-P (2.33), companied by the highest concentration of Ce^{3+}. It is demonstrated that non-equilibrium plasma coupled with calcination boosts the chemical states changing from Cu^{2+} and Ce^{4+} to Cu^{+} and Ce^{3+}, caused by the reduction effect of high energy electrons in plasma. Besides, higher ratio of Cu^{+} and Ce^{3+} in CuCe-CP owing to the strong synergy between CuO and CeO_2, resulting to a larger number of active sites Cu-[Ox]-Ce [38], which can also be attributed to the preparation method.

3.7. H_2-TPR

Fig. 5 shows the H_2-TPR results of the CuO/CeO_2 nanorod catalysts with different preparation. Since ceria can only be reduced by hydrogen above 350 °C, the reduction peaks below 350 °C are simply related to the reduction of copper species. The H_2-TPR curves in Fig. 5 can be fitted to three reduction peaks of α, β, and γ. The α and β peaks are respectively classified to the highly dispersed superficial Cu^{2+}, which have strong interactions with CeO_2, and the reduction of crystalline CuO species [29]. The γ peak represents reduction of bulk CuO particles with weak interaction associated with CeO_2. It can be seen from Table 1 that the reduction temperature of α peak for the glucose-containing catalysts obtained under different preparation conditions tends to be higher than those of glucose-free catalysts. The α peak reduction temperature of CuCe-CP is the lowest, suggesting that non-equilibrium plasma coupled with calcination is beneficial to enhance the low-temperature reducibility of the catalyst. This phenomenon can be explained by the fact that a strong electric field is formed on the catalyst surface when the catalyst is modified by non-equilibrium plasma, which can expose more active crystal planes than traditional calcination. Consequently, it further strengthens the interaction between CuO and CeO_2 and promotes the dispersion of active CuO, as has been shown by the TEM, XRD results, followed by the improved reducibility at low temperature.

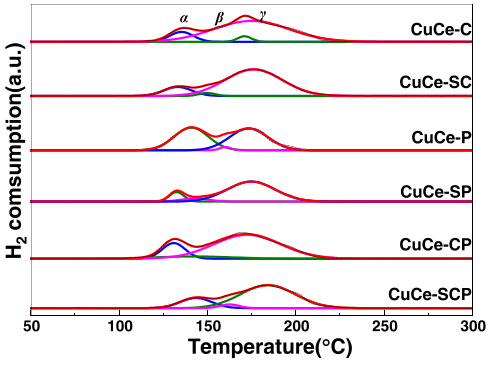

Fig. 5. H_2-TPR spectra of CuO/CeO_2 nanorod catalysts.

3.8. O_2-TPD

The adsorbed oxygen and oxygen consumption on the catalysts were deeply investigated by O_2-TPD in order to analyze the oxygen storage and oxygen release capabilities, as displayed in Fig. S3. The α and β peaks can be assigned to the physically adsorbed oxygen and chemically adsorbed oxygen on the catalyst surface, respectively. And the desorption peaks γ at high temperature are attributed to the lattice oxygen in CuO. Under the same calcination method, the β peaks of glucose-free catalysts seem to shift to low temperature compared with the glucose-containing catalysts. As proved by Raman and XPS results, the glucose-free catalysts can provide more oxygen vacancies for the chemical adsorption of oxygen, which is the consequence of high ratio of Ce^{3+} and Cu^{+} in them. Furthermore, the temperature of γ peaks of CuCe-CP is the lowest among the three glucose-free catalysts (720 ℃ for CuCe-

C, 769 ℃ for CuCe-P and 732 ℃ for CuCe-CP), indicating that Cu and Ce species in CuCe-CP have the strongest synergistic effect, which strengthens the activity of CuO lattice oxygen.

3.9. Evaluation of catalytic activity

Fig. 6 illustrates the catalytic activity of the CuO/CeO_2 nanorod catalysts towards toluene and its CO_2 selectivity. The conversion temperature of toluene oxidation over CuO/CeO_2 nanorod catalyst is shown in Table S1. T_{90} (temperature at 90% conversion rate) of all the catalysts can be listed in descending order as CuCe-CP > CuCe-SCP > CuCe-C > CuCe-SC > CuCe-P > CuCe-SP. CuCe-CP exhibits the lowest T_{90} of 272 ℃, while CuCe-SP shows the highest T_{90} of 307 ℃. Meanwhile, the CO_2 yield of CuCe-SCP and CuCe-CP catalysts is the best, reaching 100% at 260 °C, which is higher than other catalysts. With the same preparation method, the catalytic activities of the glucose-containing catalysts are distinctively lower than those of glucose-free catalysts. It is probably attributed to the incomplete decomposition of glucose or the sintering of CuO caused by the overheat generated by the decomposition of glucose during the preparation procedure, both leading to the decreasing of oxygen vacancies. Therefore, glucose-free catalysts contain more oxygen vacancies with better dispersed CuO.

It is obvious that non-equilibrium plasma treatment plays a critical role in the improvement of catalytic activity and CO_2 selectivity. The catalytic activities for glucose-free catalysts follow the order of CuCe-CP > CuCe-C > CuCe-P. It is apparent that CuCe-CP prepared by calcination coupling with non-equilibrium plasma shows the best activity. The high-energy electrons and free radicals in plasma can enhance the interaction between CuO and CeO_2 and benefit to the high dispersion of the active phase CuO (TEM and XRD) and low-temperature reducibility (H_2-TPR). Hence, CuCe-CP produces the most Ce^{3+} content under the reduction effect of non-equilibrium plasma, as shown by XPS results. Thereafter, due to the strong oxygen storage capacity of Ce^{3+}, more oxygen vacancies are generated, and the ability of adsorbing and activating gas-phase oxygen and further the catalytic activity and CO_2 selectivity are facilitated.

In summary, non-equilibrium plasma treatment towards CuO/CeO_2 can enhance the synergistic effect between Cu and Ce generating more Cu-[Ox]-Ce sites, increase the oxygen vacancy concentration in the catalysts and then promotes the ability to adsorb and activate gas-phase oxygen. Thereby the catalytic oxidation reaction of toluene is conformed to follow the Mars van Krevelen (MvK) mechanism. The proposed reaction path of CuCe-CP is shown in Fig. 7. First, toluene is adsorbed and combined with the active oxygen species on the catalyst surface (①), and then reacts with the adjacent active oxygen species on the catalyst surface to be converted into intermediate products such as benzoyl, benzoic acid, and benzaldehyde[39], which are finally converted into CO_2 and H_2O (②). The oxidation of toluene consumes the active lattice oxygen on the catalyst surface to generate oxygen vacancies, while gas-phase oxygen is adsorbed on the oxygen vacancies and is activated

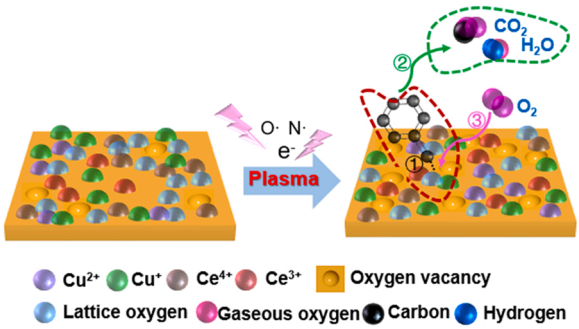

Fig. 7. Reaction pathway of toluene oxidation on CuO/CeO_2 treated by non-equilibrium plasma.

for supplementing the active oxygen species (③). During the catalytic oxidation process, the active sites Cu-[Ox]-Ce formed by the strong interaction between Cu and Ce provide a large number of oxygen vacancies, which enables the catalyst to activate gas-phase oxygen and transfer reactive oxygen species during the toluene oxidation reaction. This result can be explained by the coexistence of different chemical valences of copper species and the transformation between Cu^{2+} and Cu^{+} (by XPS). The re-dox pairs of Cu^{+}/Cu^{2+} and Ce^{3+}/Ce^{4+} can reinforce the mobility of bulk oxygen and surface oxygen in the catalyst through the electron exchange between copper and cerium ions.

4. Conclusion

Non-equilibrium plasma was adopted to prepare CuO/CeO_2 nanorod catalysts comparing with traditional calcination. The influences of non-equilibrium plasma on the catalytic performances of toluene oxidation and the physicochemical properties of the catalyst were deeply investigated based on the characterization results of XRD, TEM, H_2-TPR, O_2-TPD, XPS. After non-equilibrium plasma treatment of calcined CuO/CeO_2, the synergic effects between CuO and CeO_2 nanorod are significantly enhanced, contributing to the generation of rich oxygen vacancies and high dispersion of the CuO active phase. And the high-energy electrons and radicals in plasma improve the ratio of Cu^{+}/Cu^{2+} and Ce^{3+}/Ce^{4+} on the catalyst surface which accelerate the formation of oxygen vacancies and the mobility of active oxygen species. The rich oxygen vacancy can facilitate adsorption and activation of gaseous oxygen and it plays a positive crucial role in the catalytic oxidation of toluene. It is suggested that non-equilibrium plasma is an effective strategy to control oxygen vacancy in the catalyst.

CRediT authorship contribution statement

Jianyu Yun: The design of experiments, Carrying out experiments, Data curation, Writing – original draft preparation, Writing – review &

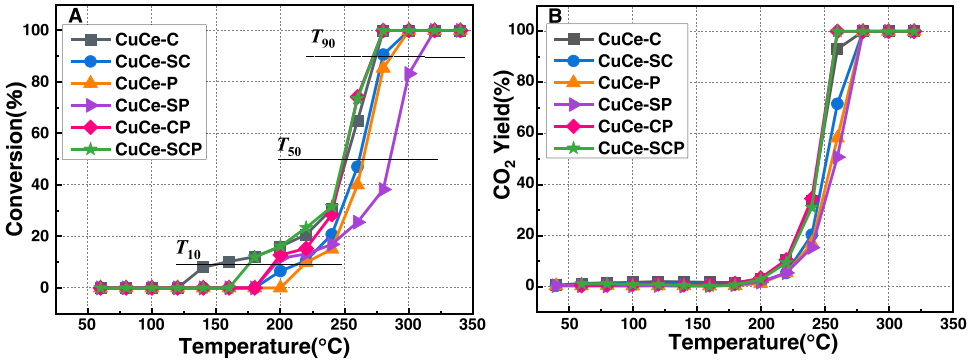

Fig. 6. Conversion (A) and CO_2 selectivity (B) of toluene oxidation over CuO/CeO_2 nanorod catalysts.

editing. **Zihao Teng**: Writing – review & editing. **Liangkai Wu**: Preparation of catalysts and carrying out experiments. **Xin Gao**: Check articles and references. **Feng Bin**: Methodology for catalyst preparation, Writing – review & editing, Acquisition of the financial support for the project leading to this publication. **Qinglan Hao**: Methodology, Supervision. **Baojuan Dou**: Writing – review & editing.

Declaration of Competing Interest

The authors declare that they have no known competing financial interests or personal relationships that could have appeared to influence the work reported in this paper.

Acknowledgments

We gratefully thank the financial support from the Tianjin Municipal Natural Science Foundation (19JCZDJC40100) and the Guangxi Key Research and Development Program (2021AB25028).

Appendix A. Supporting information

Supplementary data associated with this article can be found in the online version at doi:10.1016/j.jece.2022.107847.

References

[1] M.S. Kamal, S.A. Razzak, M.M. Hossain, Catalytic oxidation of volatile organic compounds (VOCs) - A review, Atmos. Environ. 140 (2016) 117–134, https://doi.org/10.1016/j.atmosenv.2016.05.031.
[2] C.T. Yang, G. Miao, Y.H. Pi, Q.B. Xia, J.L. Wu, Z. Li, J. Xiao, Abatement of various types of VOCs by adsorption/catalytic oxidation: A review, Chem. Eng. J. 370 (2019) 1128–1153, https://doi.org/10.1016/j.cej.2019.03.232.
[3] Y.S. Son, Decomposition of VOCs and odorous compounds by radiolysis: A critical review, Chem. Eng. J. 316 (2017) 609–622, https://doi.org/10.1016/j.cej.2017.01.063.
[4] S. Aguado, A.C. Polo, M.P. Bernal, J. Coronas, J. Santamaria, Removal of pollutants from indoor air using zeolite membranes, J. Membr. Sci. 240 (1–2) (2004) 159–166, https://doi.org/10.1016/j.memsci.2004.05.004.
[5] Y.H. Pi, X.Y. Li, Q.B. Xia, J.L. Wu, Y.W. Li, J. Xiao, Z. Li, Adsorptive and photocatalytic removal of Persistent Organic Pollutants (POPs) in water by metal-organic frameworks (MOFs), Chem. Eng. J. 337 (2018) 351–371, https://doi.org/10.1016/j.cej.2017.12.092.
[6] Z.X. Zhang, Z. Jiang, W.F. Shangguan, Low-temperature catalysis for VOCs removal in technology and application: A state-of-the-art review, Catal. Today 264 (2016) 270–278, https://doi.org/10.1016/j.cattod.2015.10.040.
[7] R.N. Kang, J.Q. Huang, F. Bin, Z.H. Teng, X.L. Wei, B.J. Dou, S. Kasipandi, Evolution behavior and active oxygen quantification of reaction mechanism on cube Cu2O for CO self-sustained catalytic combustion and chemical-looping combustion, Appl. Catal. B. 310 (2022), 121296, https://doi.org/10.1016/j.apcatb.2022.121296.
[8] W.J. Liang, X. Li, H.L. Ju, S.D. Ren, Adsorption and dissociation mechanism of toluene on Pd(111) and PdO(101) surface: First pri nciple calculation, Surf. Sci. 720 (2022), 122051, https://doi.org/10.1016/j.susc.2022.122051.
[9] H. Wang, W. Yang, P.H. Tian, J. Zhou, R. Tang, S.J. Wu, A highly active and anti-coking Pd-Pt/SiO_2 catalyst for catalytic combustion of toluene at low temperature, Appl. Catal. A: Gen. 529 (2017) 60–67, https://doi.org/10.1016/j.apcata.2016.10.016.
[10] S. Zhao, K.Z. Li, S. Jiang, J.H. Li, Pd-Co based spinel oxides derived from pd nanoparticles immobilized on layered double hydroxides for toluene combustion, Appl. Catal. B 181 (2016) 236–248, https://doi.org/10.1016/j.apcatb.2015.08.001.
[11] W.T. Zhao, Y.Y. Zhang, X.W. Wu, Y.Y. Zhan, X.Y. Wang, C.T. Au, L.L. Jiang, Synthesis of Co-Mn oxides with double-shelled nanocages for low-temperature toluene combustion, Catal. Sci. Technol. 8 (17) (2018) 4494–4502, https://doi.org/10.1039/C8CY01206G.
[12] P.M. Kouotou, G.F. Pan, J.J. Weng, S.B. Fan, Z.Y. Tian, Stainless steel grid mesh-supported CVD made Co_3O_4 thin films for catalytic oxidation of VOCs of olefins type at low temperature, J. Ind. Eng. Chem. 35 (2016) 253–261, https://doi.org/10.1016/j.jiec.2015.12.039.
[13] Z. Abbasi, M. Haghighi, E. Fatehifar, S. Saedy, Synthesis and physicochemical characterizations of nanostructured Pt/Al_2O_3-CeO_2 catalysts for total oxidation of VOCs, J. Hazard. Mater. 86 (2–3) (2011) 1445–1454, https://doi.org/10.1016/j.jhazmat.2010.12.034.
[14] C.Q. Hu, Q.S. Zhu, Z. Jiang, Y.Y. Zhang, Y. Wang, Preparation and formation mechanism of mesoporous CuO-CeO_2 mixed oxides with excellent catalytic performance for removal of VOCs, Micro Mesopor. Mat. 113 (1–3) (2008) 427–434, https://doi.org/10.1016/j.micromeso.2007.11.043.
[15] P. Yang, Z.N. Shi, S.S. Yang, R.X. Zhou, High catalytic performances of CeO_2-CrOx catalysts for chlorinated VOCs elimination, Chem. Eng. 126 (2015) 361–369, https://doi.org/10.1016/j.ces.2014.12.051.
[16] S. Somekawa, T. Hagiwara, K. Fujii, M. Kojima, T. Shinoda, K. Takanabe, K. Domen, Mineralization of volatile organic compounds (VOCs) over the catalyst CuO-Co_3O_4-CeO_2 and its applications in industrial odor control, Appl. Catal. A: Gen. 409–410 (2011) 209–214, https://doi.org/10.1016/j.apcata.2011.10.004.
[17] P. Yang, S.S. Yang, Z.N. Shi, Z.H. Meng, R.X. Zhou, Deep oxidation of chlorinated VOCs over CeO_2 -based transition metal mixed oxide catalysts, Appl. Catal. B. 162 (2015) 227–235, https://doi.org/10.1016/j.apcatb.2014.06.048.
[18] C. He, Y.K. Yu, L. Yue, N.L. Qiao, J.J. Li, Q. Shen, W.J. Yu, J.S. Chen, Z.P. Hao, Low-temperature removal of toluene and propanal over highly active mesoporous CuCeOx catalysts synthesized via a simple self-precipitation protocol, Appl. Catal. B. 147 (2014) 156–166, https://doi.org/10.1016/j.apcatb.2013.08.039.
[19] C. He, Y.K. Yu, Q. Shen, J.S. Chen, N.L. Qiao, Catalytic behavior and synergistic effect of nanostructured mesoporous CuO-MnOx-CeO_2 catalysts for chlorobenzene destruction, Appl. Surf. 297 (2014) 59–69, https://doi.org/10.1016/j.apsusc.2014.01.076.
[20] C. He, B.T. Xu, J.W. Shi, N.L. Qiao, Z.P. Hao, J.L. Zhao, Catalytic destruction of chlorobenzene over mesoporous ACeOx(A = Co, Cu, Fe, Mn, or Zr) composites prepared by inorganic metal precursor spontaneous precipitation, Fuel Process. Technol. 130 (2015) 179–187, https://doi.org/10.1016/j.fuproc.2014.10.008.
[21] B.J. Dou, R.Z. Zhao, N.N. Yan, C.C. Zhao, Q.L. Hao, K.S. Hui, K.N.N. Hui, A facilitated synthesis of hierarchically porous Cu–Ce–Zr catalyst using bacterial cellulose for VOCs oxidation, Mater. Chem. Phys. 237 (C) (2019), 121852, https://doi.org/10.1016/j.matchemphys.2019.121852.
[22] P.H.A. Nobrega, V. Rohani, L. Fulcheri, Non-thermal plasma treatment of volatile organic compounds: A predictive model based on experimental data analysis, Chem. Eng. J. 364 (2019) 37–44, https://doi.org/10.1016/j.cej.2019.01.100.
[23] L.B. Di, J.S. Zhang, X.L. Zhang, A review on the recent progress, challenges, and perspectives of atmospheric-pressure cold plasma for preparation of supported metal catalysts, Plasma Process. Polym. 15 (5) (2018), e1700234, https://doi.org/10.1002/ppap.201700234.
[24] M.B. Zhang, X.L. Zhu, X. Liang, Z. Wang, Preparation of highly efficient Au/C catalysts for glucose oxidation via novel plasma reduction, Catal. Commun. 25 (2012) 92–95, https://doi.org/10.1016/j.catcom.2012.04.012.
[25] H. Sun, Z.G. Liu, S. Chen, X. Quan, The role of lattice oxygen on the activity and selectivity of the OMS-2 catalyst for the total oxidation of toluene, Chem. Eng. J. 270 (2015) 58–65, https://doi.org/10.1016/j.cej.2015.02.017.
[26] K.I. Hadjiivanov, Identification of Neutral and Charged N_xO_y Surface Species by IR Spectroscopy, Catal. Rev. Sci. Eng. 42 (1–2) (2000) 71–144, https://doi.org/10.1081/CR-100100260.
[27] D.D. Miller, S.S.C. Chuang, In situ infrared study of NO reduction over Pd/Al_2O_3 and Ag-Pd/Al_2O_3 catalysts under H_2-rich and lean-burn conditions, J. Taiwan Inst. Chem. E. 40 (6) (2009) 613–621, https://doi.org/10.1016/j.jtice.2009.04.006.
[28] C. Norsic, J.M. Tatibouet, C. Batiot-Dupeyrat, E. Fourre, Non thermal plasma assisted catalysis of methanol oxidation on Mn, Ce and Cu oxides supported on γ-Al_2O_3, Chem. Eng. J. 304 (2016) 563–572, https://doi.org/10.1016/j.cej.2016.06.091.
[29] Y.Q. Zeng, K.G. Haw, Z.G. Wang, Y.A. Wang, S.L. Zhang, P. Hongmanorom, Q. Zhong, S. Kawi, Double redox process to synthesize CuO–CeO_2 catalysts with strong Cu–Ce interaction for efficient toluene oxidation, J. Hazard. Mater. 404 (A) (2021), 124088, https://doi.org/10.1016/j.jhazmat.2020.124088.
[30] W.L. Yang, D. Li, D.M. Xu, X.Y. Wang, Effect of CeO_2 preparation method and Cu loading on CuO/CeO_2 catalysts for methane combustion, J. Nat. Gas. Chem. 18 (04) (2009) 458–466, https://doi.org/10.1016/S1003-9953(08)60141-3.
[31] C.Y. Xu, P.X. Zhang, L. Yan, Blue shift of Raman peak from coated TiO_2 nanoparticles, J. Raman Spectrosc. 32 (10) (2001) 862–865, https://doi.org/10.1002/jrs.773.
[32] L. Qi, Q. Yu, Y. Dai, C.J. Tang, L.J. Liv, H.L. Zhang, F. Gao, L. Dong, Y. Chen, Influence of cerium precursors on the structure and reducibility of mesoporous CuO-CeO_2 catalysts for CO oxidation, Appl. Catal. B. 119 (2012) 308–320, https://doi.org/10.1016/j.apcatb.2012.02.029.
[33] H.H. Liu, Y. Wang, A.P. Jia, S.Y. Wang, M.F. Luo, J.Q. Lu, Oxygen vacancy promoted CO oxidation over Pt/CeO_2 catalysts: A reaction at Pt-CeO_2 interface, Appl. Surf. Sci. 314 (2014) 725–734, https://doi.org/10.1016/j.apsusc.2014.06.196.
[34] T. Kang, B. Li, Q.L. Hao, W.J. Gao, F. Bin, K.N. Hui, D. Fu, B.J. Dou, Efficient Hydrogen Peroxide (H_2O_2) Synthesis by $CaSnO_3$ via Two-Electron Water Oxidation Reaction, ACS Sustain. Chem. Eng. 8 (39) (2020) 15005–15012, https://doi.org/10.1021/acssuschemeng.0c05449.
[35] D. Delimaris, T. Ioannides, VOC oxidation over CuO–CeO_2 catalysts prepared by a combustion method, Appl. Catal. B. 89 (1) (2009) 295–302, https://doi.org/10.1016/j.apcatb.2009.02.003.
[36] X.L. Pang, H.Y. Bai, D.B. Xu, J.R. Ding, W.Q. Fan, W.D. Shi, Dual-functional electrochemical bio-sensor built from Cu_2O for sensitively detecting the thiols and Hg^{2+}, APPL SURF SCI 564 (2021), 150397 https://doi.org/10.1016/j.apsusc.2021.150397.
[37] S.B. Wang, H.J. Yang, X.Y. Yi, H.M.K. Sari, X. Zhang, T. Wang, Z.Y. Zhou, B. Cao, J. Qin, J.J. Wang, W.B. Li, X.F. Li, Significant influence of controllable surface

oxygen vacancies of CuO for enhancing sensitivity of glucose detection, APPL SURF SCI 574 (2022), 151649, https://doi.org/10.1016/j.apsusc.2021.151649.
[38] L. Li, C.Y. Zhang, F. Chen, Y.T. Xiang, J.L. Yan, W. Chu, Facile fabrication of hollow structured Cu-Ce binary oxides and their catalytic properties for toluene combustion, Catal. Today. 376 (2020) 239–246, https://doi.org/10.1016/j.cattod.2020.05.038.
[39] B.J. Dou, S.M. Li, D.L. Liu, R.Z. Zhao, J.G. Liu, Q.L. Hao, F. Bin, Catalytic oxidation of ethyl acetate and toluene over Cu–Ce–Zr supported ZSM-5/TiO_2 catalysts, RSC Adv. 6 (59) (2016) 53852–53859, https://doi.org/10.1039/C6RA06421C.